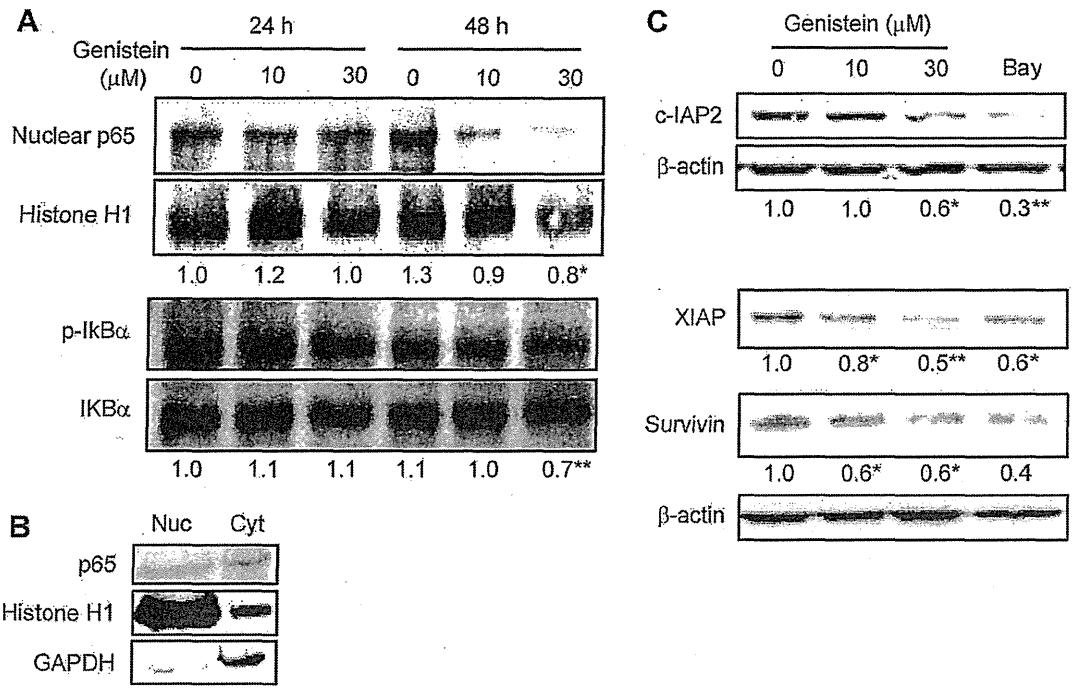

Figure 3 Genistein ameliorates overactivation of the NF-κB pathway. (A) Cells were treated with 0, 10 and 30 μM genistein for 24 and 48 h, and nuclear p65, histone H1, phosphorylated IκBα (p-IκBα) and β-actin were detected using Western blot analysis. (C) Cells were treated with 0, 10 and 30 μM genistein or 1 μM Bay11-7082 (Bay) for 48 h, and then c-IAP2, XIAP, survivin and β-actin were detected using Western blot analysis. Numbers represent the mean values of the quantified band intensities for three independent experiments. Representative blot patterns are shown. Numbers marked with asterisks are significant with respect to the control at $^*P < 0.05$ and $^{**}0.01$. (B) p65, histone H1 and GAPDH detection in cytosolic and nuclear fraction to confirm no contamination between subcellular fractions. Nuc, nuclear fraction; Cyt, cytosolic fraction.

genistein, which suggests that PARP activation and the resulting AIF-mediated apoptosis at least partially contribute to the cytotoxicity of genistein.

The HTLV-I viral protein, Tax, activates the expression of several genes through NF-κB, which results in deregulated cell proliferation and resistance to apoptosis (Taylor and Nicot, 2008; Saggioro et al., 2009). XIAP and surviving, which are anti-apoptotic proteins, and NF-κB responsive genes are abundantly expressed in HTLV-1-infected T-cell lines (Mori et al., 2001; Mohapatra et al., 2003). Under steady-state conditions, NF-κB in an inactive form is localised to the cytoplasm by association with the IκB subunit; activation of NF-κB involves the phosphorylation and degradation of IκB NF-κB pathway is activated in primary ATL cells (Mori et al., 1999), a pathway that has received attention as a target for new drugs. Bay11-7082 and DHMEQ, both potent NF-κB inhibitors, strongly induce apoptosis of HTLV-I transfected and ATL cells (Mori et al., 2002; Ohsugi et al., 2005, 2006). Our data show that genistein inhibits p65 translocation into the nucleus and suppresses the expression of c-IAP2, XIAP and survivin. In contrast, although inhibition of p65 translocation and IκBα phosphorylation were not seen after 24 h of genistein treatment, apoptosis was seen at 24 h, suggesting that an NF-κB-dependent pathway is involved in the promotion of apoptosis.

Since genistein has a striking ability to induce accumulation of p53 protein (Yamasaki et al., 2007), it is noteworthy that the majority of HTLV-1-infected cells and also in Hut102 cells, wild-type p53 is present, but in a functionally inactive state. Because strategies to recover p53 activity in ATL cells are now focused on the molecular targets of ATL (Jung et al., 2008), further studies are necessary to elucidate the molecular mechanisms underlying the mode of action of genistein, particularly those related to p53 function and the NF-κB pathway in ATL cells.

Funding

Funding for this project was partially provided by Mishima Kaiun Memorial Foundation 2009.

References

Baxa DM, Luo X, Yoshimura FK (2005) Genistein induces apoptosis in T lymphoma cells via mitochondrial damage. Nutr Cancer 51: 93–101.

Chang KL, Kung ML, Chow NH Su SJ (2004) Genistein arrests hepatoma cells at G2/M phase: involvement of ATM activation and upregulation of p21waf/1cip1 and Wee1. Biochem Pharmacol 67: 717–26.

Hanchard B, Gibbs WN, Lofters W, Campbell M, Williams E, Williams N, Jaffe E, Cranston B, Panchoosingh LD, LaGrenade L, Wilks R, Murphy E, Blattner W, Manns A (1990) HTLV. In: Blattner WA, ed. *Human retrovirology.* New York: Raven Press, pp. 173–83.

Haneji K, Matsuda T, Tomita M, Kawakami H, Ohshiro K, Uchihara JN, Masuda M, Takasu N, Tanaka Y, Ohta T, Mori N (2005) Fucoidan extracted from *Cladosiphon okamuranus* Tokida induces apoptosis of human T-cell leukemia virus type 1-infected T-cell lines and primary adult T-cell leukemia cells. Nutr Cancer 52: 189–201.

Hewitt AL, Singletary KW (2003) Soy extract inhibits mammary adenocarcinoma growth in a syngeneic mouse model. Cancer Lett 192: 133–43.

Jung KJ, Dasgupta A, Huang K, Jeong SJ, Pise-Masison C, Gurova KV, Brady JN (2008) Small-molecule inhibitor which reactivates p53 in human T-cell leukemia virus type 1-transformed cells. J Virol 82: 8537–47.

Karmakar S, Choudhury SR, Banik NL, Ray SK (2009) Combination of N-(4-hydroxyphenyl) retinamide and genistein increased apoptosis in neuroblastoma SK-N-BE2 and SH-SY5Y xenografts. Neuroscience 163: 286–95.

Li W, Frame LT, Hoo KA, Li Y, D'Cunha N, Cobos E (2011) Genistein inhibited proliferation and induced apoptosis in acute lymphoblastic leukemia, lymphoma and multiple myeloma cells in vitro. Leuk Lymphoma 52: 2380–90.

Liao CH, Pan SL, Guh JH, Teng CM (2004) Genistein inversely affects tubulin-binding agent-induced apoptosis in human breast cancer cells. Biochem Pharmacol 67: 2031–8.

Mohan N, Karmakar S, Choudhury SR, Banik NL, Ray SK (2009) Bcl-2 inhibitor HA 14-1 and genistein together adeptly down regulated survival factors and activated cysteine proteases for apoptosis in human malignant neuroblastoma SK-N-BE2 and SH-SY5Y cells. Brain Res 1283: 155–66.

Mohapatra S, Chu B, Wei S, Djeu J, Epling-Burnette PK, Loughran T, Jove R, Pledger WJ (2003) Roscovitine inhibits STAT5 activity and induces apoptosis in the human leukemia virus type 1-transformed cell line MT-2. Cancer Res 63: 8523–30.

Mori N, Yamada Y, Ikeda S, Yamasaki Y, Tsukasaki K, Tanaka Y, Tomonaga M, Yamamoto N, Fujii M (1999) Constitutive activation of NF-kappaB in primary adult T-cell leukemia cells. Blood 93: 2360–8.

Mori N, Yamada Y, Hata T, Ikeda S, Yamasaki Y, Tomonaga M, Yamamoto N (2001) Expression of survivin in HTLV-I-infected T-cell lines and primary ATL cells. Biochem Biophys Res Commun 282: 1110–3.

Mori N, Yamasa Y, Ikeda S, Yamasaki Y, Tsukasaki K, Tanaka Y, Tomonaga M, Yamamoto N, Fujii M (2002) Bay 11-7082 in hibits transcription factor NF-kappaB and induces apoptosis of HTLV-I–infected T-cell lines and primary adult T-cell leukemia cells. Blood 100: 1828–34.

Ohsugi T, Horie R, Kumasaka T, Ishida A, Ishida T, Yamaguchi K, Watanabe T, Umezawa K, Urano T (2005) In vivo antitumor activity of the NF-kappaB inhibitor dehydroxymethylepoxyquinomicin in a mouse model of adult T-cell leukemia. Carcinogenesis 26: 1382–8.

Ohsugi T, Kumasaka T, Ishida A, Ishida T, Horie R, Watanabe T, Umezawa K, Yamaguchi K (2006) In vitro and in vivo antitumor activity of the NF-kappaB inhibitor DHMEQ in the human T-cell leukemia virus type I-infected cell line, HUT-102. Leuk Res 30: 90–7.

Saggioro D, Silic-Benussi M, Biasiotto R, D'Agostino DM, Ciminale V (2009) Control of cell death pathways by HTLV-I proteins. Front Biosci 14: 3338–51.

Su SJ, Chow NH, Kung ML, Hung TC, Chang KL (2003) Effects of soy isoflavones on apoptosis induction and G2-M arrest in human hepatoma cells involvement of caspase-3 activation, Bcl-2 and Bcl-XL downregulation, and Cdc2 kinase activity. Nutr Cancer 45: 113–23.

Taylor JM, Nicot C (2008) HTLV-1 and apoptosis: role in cellular transformation and recent advances in therapeutic approaches. Apoptosis 13: 733–47.

Tomita M, Kawakami H, Uchihara JN, Okudaira T, Masuda M, Takasu N, Matsuda T, Ohta T, Tanaka Y, Ohshiro K, Mori N (2006) Curcumin (diferuloylmethane) inhibits constitutively active NF-kappaB, leading to suppression of cell growth of human T-cell leukemia virus type I-infected T-cell lines and primary adult T-cell leukemia cells. Int J Cancer 118: 765–72.

Tomita M, Kawakami H, Uchihara JN, Okudaira T, Masuda M, Takasu N, Matsuda T, Ohta T, Tanaka Y (2006) Curcumin suppresses constitutive activation of AP-1 by downregulation of Jun D protein in HTLV-1-infected T-cell lines. Leuk Res 30: 313–21.

Yamaguchi K, Kiyokawa T, Futami G, Ishii T, Takatsuki K (1990) HTLV. In: Blattner WA, ed. *Human retrovirology.* New York: Raven Press, pp. 163–71.

Yamasaki M, Fujita S, Ishiyama E, Mukai A, Madhyastha H, Sakakibara Y, Suiko M, Hatakeyama K, Nemoto T, Morishita K, Kataoka H, Tsubouchi H, Nishiyama K (2007) Soy derived isoflavones inhibit the growth of adult T-cell leukemia cells in vitro and in vivo. Cancer Sci 98: 1740–6.

Yu SW, Andrabi SA, Wang H, Kim NS, Poirier GG, Dawson TM, Dawson VL (2006) Apoptosis-inducing factor mediates poly (ADP-ribose) (PAR) polymer-induced cell death. Proc Natl Acad Sci USA 103: 18314–9.

Yu SW, Wang H, Poitras MF, Coombs C, Bowers WJ, Federoff HJ, Poirier GG, Dawson TM, Dawson VL (2002) Mediation of poly (ADP-ribose) polymerase-1-dependent cell death by apoptosis-inducing factor. Science 297: 259–63.

Zhang J, Nagasaki M, Tanaka Y, Morikawa S (2003) Capsaicin inhibits growth of adult T-cell leukemia cells. Leuk Res 27: 275–83.

Received 18 October 2012; accepted 22 February 2013.
Final version published online 18 April 2013.

Leukemia (2013) 27, 1637–1649

www.nature.com/leu

ORIGINAL ARTICLE

Maintenance of the hematopoietic stem cell pool in bone marrow niches by EVI1-regulated GPR56

Y Saito[1], K Kaneda[1], A Suekane[1], E Ichihara[1], S Nakahata[1], N Yamakawa[1], K Nagai[1], N Mizuno[2], K Kogawa[3], I Miura[4], H Itoh[2] and K Morishita[1]

Acute myeloid leukemia with high ecotropic viral integration site-1 expression (EVI1^{high} AML) is classified as a refractory type of leukemia with a poor prognosis. To provide new insights into the prevention and treatment of this disease, we identified the high expression of EVI1-regulated G protein-coupled receptor 56 (GPR56), and the association of high cell adhesion and antiapoptotic activities in EVI1^{high} AML cells. Knockdown of GPR56 expression decreased the cellular adhesion ability through inactivation of RhoA signaling, resulting in a reduction of cellular growth rates and enhanced apoptosis. Moreover, in *Gpr56*$^{-/-}$ mice, the number of hematopoietic stem cells (HSCs) was significantly decreased in the bone marrow (BM) and, conversely, was increased in the spleen, liver and peripheral blood. The number of *Gpr56*$^{-/-}$ HSC progenitors in the G0/G1-phase was significantly reduced and was associated with impaired cellular adhesion. Finally, the loss of GPR56 function resulted in a reduction of the *in vivo* repopulating ability of the HSCs. In conclusion, GPR56 may represent an important GPCR for the maintenance of HSCs by acting as a co-ordinator of interactions with the BM osteosteal niche; furthermore, this receptor has the potential to become a novel molecular target in EVI1^{high} leukemia.

Leukemia (2013) **27**, 1637–1649; doi:10.1038/leu.2013.75

Keywords: acute myeloid leukemia; EVI1; GPR56; hematopoietic stem cell; RhoA

INTRODUCTION

Acute myeloid leukemia (AML) is a cancer of the myeloid line of blood cells, and refractory AML is considered a stem cell disease. Leukemia stem cells (LSCs) are thought to be the hijack maintenance mechanisms of hematopoietic stem cells (HSCs) in the bone marrow (BM), and consequently to contribute to eventual disease relapse after they have survived undetected in the BM niche during chemotherapy.[1,2] Therefore, if the adhesion molecules specific for LSC maintenance in the BM niche can be found, targeting these interaction molecules between LSC and the surrounding support cells could represent a promising and novel therapeutic strategy for AML.

The ecotropic viral integration site-1 (EVI1) transcription factor is a well-known marker of poor prognosis for chemotherapy-resistant AML.[3–8] The gene expression profiles found in acute myeloid leukemia with high ecotropic viral integration site-1 expression (EVI1^{high} AML) patients are quite similar to those of BM CD34^{+} cells;[9,10] EVI1 is implicated in stem cell regulation and oncogenesis, and contributes to the poor clinical outcome of AML by promoting stemness.[11] EVI1 maintains the self-renewal capacity of embryonic HSCs by activating Gata2 transcription,[12] and the ablation of EVI1 in adult BM leads to a significant decrease in the numbers of HSCs.[13] Therefore, EVI1 may have an important role in the maintenance of cell quiescence and stem cell-like phenotypes in leukemia cells, thereby contributing to their chemoresistance.

To identify novel therapeutic molecules targeting EVI1^{high} AML cells, we analyzed the gene expression profiles of these molecules and the newly identified G protein-coupled receptor 56 (GPR56) as a candidate target molecule for EVI1^{high} AML cells, along with CD52, integrin α6 and Angiopoietin-1.[14–16] GPR56 is a member of the secretin family and has been linked to developmental malformations of the human brain, known as bilateral frontoparietal polymicrogyria.[17–19] GPR56, coupled with $G\alpha_{12/13}$, induces Rho-dependent activation of transcription, resulting in actin fiber reorganization and inhibition of neural progenitor cell migration.[20] In cancer cells, overexpression of GPR56 can suppress tumor growth and metastasis in melanoma cell lines, and GPR56 functions in tumor cell adhesion in glioma cells.[21–23] Although the function of GPR56 in HSCs is still unknown,[24] GPR56 was also identified in a family of LSC-related genes correlated with a worse prognosis of AML.[11] GPR56 regulates RhoA signaling involved in cellular adhesion, and the small GTPases Rac and Cdc42 control HSC adhesion, migration and mobilization in BM niches;[25–30] therefore, we speculated that GPR56 has an important role in the maintenance of HSCs and/or LSCs in the BM niche.

In this study, we found that GPR56 was specifically expressed in EVI1^{high} AML cells as an EVI1-targeted gene and was associated with high cell adhesion and antiapoptotic activities in the leukemia cells. To further define the role of GPR56 in HSC regulation, we analyzed the function of HSCs in *Gpr56*$^{-/-}$ mice, and our results demonstrated a role of Gpr56 in maintaining HSC quiescence and osteosteal niche interactions in the BM. Because the expression of GPR56 in LSCs is higher than in HSCs, GPR56 has potential as a novel therapeutic target for EVI1^{high} AML.

[1]Division of Tumor and Cellular Biochemistry, Department of Medical Science, Faculty of Medicine, University of Miyazaki, Miyazaki, Japan; [2]Laboratory of Molecular Signal Transduction, Graduate School of Biological Sciences, Nara Institute of Science and Technology, Nara, Japan; [3]Department of Pediatrics, National Defense Medical College, Tokorozawa, Japan and [4]Division of Hematology and Oncology, Department of Internal Medicine, St Marianna University School of Medicine, Kawasaki, Japan. Correspondence: Dr K Morishita, Division of Tumor and Cellular Biochemistry, Department of Medical Science, Faculty of Medicine, University of Miyazaki, 5200 Kihara, Kiyotake, Miyazaki 889-1692, Japan.
E-mail: kmorishi@med.miyazaki-u.ac.jp
Received 15 October 2012; revised 4 March 2013; accepted 6 March 2013; accepted article preview online 12 March 2013; advance online publication, 5 April 2013

MATERIALS AND METHODS

Cell lines

UCSD/AML1 and HNT34 cells were cultured in RPMI1640 (Roswell Park Memorial Institute medium) supplemented with 10% fetal calf serum and 1 ng/ml of human granulocyte-macrophage (GM) colony-stimulating factor. U937 and K562 cells were cultured in RPMI1640 supplemented with 10% fetal calf serum, and 293T cells were cultured in Dulbecco's modified eagle medium supplemented with 10% fetal calf serum. Detailed information concerning our cell lines is available as described previously.[14]

Patient samples

Leukemia cells were obtained from AML patients before chemotherapy. A summary of the AML patient samples used in this study is presented in Supplementary Table 1. One sample with high expression of EVI1, consisting of PT9 cells, was cultured in RPMI1640 supplemented with 10% fetal calf serum and 1 ng/ml granulocyte-macrophage colony-stimulating factor.[14] This study was approved by the Institutional Review Board of the Faculty of Medicine of the University of Miyazaki. Informed consent was obtained from all donors in accordance with the Declaration of Helsinki.

Quantitative real-time reverse-transcription PCR

After extraction of total RNA using the TRIzol reagent (Invitrogen, Carlsbad, CA, USA), 1 μg of total RNA was reverse transcribed to produce complementary DNA using Reverse Transcriptase XL (AMV, avian myeloblastosis virus) (Takara-Bio Inc., Tokyo, Japan). The resulting first-strand complementary DNA was used as a template for real-time PCR. Real-time PCR was performed using MESA GREEN qPCR MasterMix Plus for SYBR assay (EUROGENTEC, Seraing, Belgium). The primers used in these experiments are listed in Supplementary Table 2. The mRNA expression levels of several genes were detected using an ABI Prism 7000 (Applied Biosystems, Foster City, CA, USA), and the data obtained were analyzed with Sequence Detection System software (Applied Biosystems) and normalized to β-actin.

Mice

Gpr56$^{-/-}$ mice were kindly provided by Genentech (South San Francisco, CA, USA).[18,19,31] C57BL/6 CD45.1 congenic mice (B6-CD45.1) were purchased from Sankyo-Lab Service (Tsukuba, Japan). For analysis of blood counts, peripheral blood (PB) from the tail vein was collected in a heparinized microtube and analyzed on a hematology analyzer (CellTac, NIHON KOHDEN, Tokyo, Japan).

Isolation of murine HSCs and flow cytometry

BM was collected from femurs and tibiae. Lin$^+$ cells were removed by immunomagnetic selection using AutoMACS magnetic-activated cell separation (Auto MACS, Miltenyi Biotec, Bergisch, Gladbach, Germany). Lin$^-$ cells were enriched for cells expressing c-Kit using Miltenyi CD117 microbeads and an AutoMACS magnetic selection device. The HSCs and myeloid progenitors were sorted by first staining Lin$^-$ BM cells with Alexa Fluor 647-conjugated anti-CD34 (RAM34; BD Bioscience, Franklin Lakes, NJ, USA), PerCP-Cy5.5-conjugated anti-CD16/32 (93; eBioscience, San Diego, CA, USA), PE-Cy5-conjugated anti-Flk2 (A2F10; eBioscience) and biotinylated anti-mGpr56 antibodies, followed by streptavidin-Allophycocyanin (APC)/Cy7 (BioLegend, San Diego, CA, USA). A rabbit anti-mGpr56 antibody was used as described previously.[20] Cells were then sorted using a JSAN cell sorter (Bay bioscience, Kobe, Japan).

RESULTS

High expression of GPR56 in EVI1^{high} AML cells

To search for novel molecular targets for EVI1^{high} AML, we recently analyzed the gene expression profiles of 12 human myeloid cell lines using an oligonucleotide microarray; from this analysis, GPR56 was identified.[14,15] In the present study, we focused on the analysis of GPR56, an orphan G protein-coupled receptor. Initially, we used quantitative real-time PCR to measure the expression of *EVI1* and *GPR56* in a panel of leukemia cell lines and primary leukemia samples (Figures 1a and b). Our results revealed that *GPR56* mRNA was significantly more highly expressed in the EVI1^{high} leukemia cell lines and patient samples than in their EVI1^{low} counterparts ($P<0.05$), and the expression of *GPR56* was highly correlated with the expression of *EVI1* (Figures 1a and b). Furthermore, based on gene expression profiles from a large number of patients with AML ($n=460$) (accession number GSE6891),[10] *GPR56* was highly expressed in EVI1^{high} AML cells compared with EVI1^{low} AML cells (Supplementary Figure 1a). In addition, the *GPR56* mRNA level associated with intermediate- and high-risk AML samples was significantly higher than that in the low-risk AML samples (Supplementary Figure 1b), suggesting that *GPR56* expression is a marker of poor prognosis in AML patients.

The expression of GPR56 was regulated by the EVI1 transcription factor

To determine whether the expression of *GPR56* is regulated by EVI1, we introduced an expression vector for EVI1-specific (shEVI1) or non-specific small hairpin RNA (shCNTL) into EVI1^{high} UCSD/AML1 and PT9 cells to establish UCSD/AML1 and PT9 cells exhibiting EVI1^{low} expression (UCSD/AML1/shEVI1, PT9/shEVI1) and control cells (UCSD/AML1/shCNTL, PT9/shCNTL). The expression of *GPR56* was significantly reduced in the UCSD/AML1/shEVI1 and PT9/shEVI1 cells compared with *GPR56* expression in parental and control cells (Figures 1c–e and Supplementary Figure 2). By contrast, the introduction of an EVI1 expression vector into U937 cells expressing EVI1^{low} produced U937 cells showing EVI1^{high} expression (U937/EVI1). The expression of *GPR56* was significantly increased in U937/EVI1 cells compared with control parental and U937/Mock cells (Figures 1f–h). To determine whether EVI1 regulates GPR56 expression, we next isolated a 3-kb fragment from the genomic promoter region of *GPR56* and inserted it in front of the firefly luciferase gene (pGL4-3.0). We created promoter DNA deletion mutants by deleting the region up to −1.5 (pGL4-1.5) or −2.4 (pGL4-2.4) kb, and the promoter activity was determined via luciferase assays after transfection into COS7 cells (Figure 2a). We found that the region between −2.4 and −3.0 kb markedly enhanced the promoter activity of *GPR56* in the presence of transfected EVI1. In addition, a possible binding sequence for the second DNA-binding domain of EVI1, GAAGAT, was found in the region between −2.4 and −3.0 kb. This binding sequence was replaced with the nucleotide sequence CCCGAC in the pGL4-3.0 plasmid (pGL4-3.0 m), and the resultant mutant plasmid completely abolished *GPR56* transcriptional activity. To confirm the DNA-binding activity of EVI1, several EVI1 deletion mutants were transfected into COS7 cells, and their *GPR56* transcriptional activity was measured (Figure 2b). The transcriptional activity of the mutant containing a deletion of the repression domain (ΔRD) showed less than half of the wild-type activity, and deletion of the second DNA-binding domain along with the eighth through the tenth zinc finger repeats (ΔD2 (8–10)) completely abolished *GPR56* transcriptional activity. In addition, the ΔD2 (8–10) EVI1 mutant protein was not precipitated by the DNA fragment of the GPR56 promoter region in chromatin immunoprecipitation assays (Figure 2c). Finally, the endogenous EVI1 protein was precipitated from UCSD/AML1 cells using the same GPR56 promoter region with the EVI1-binding site via chromatin immunoprecipitation with an anti-EVI1 antibody (Figure 2d). Therefore, EVI1 binds directly to the promoter region of *GPR56* and regulates *GPR56* expression in EVI1^{high} leukemia cells.

GPR56 regulated cell adhesion and migration in EVI1^{high} AML cells

Because high expression of GPR56 promotes tumorigenesis by enhancing the cellular adhesion of glioma cells,[21] we next compared the cell migration and adhesion abilities of leukemia

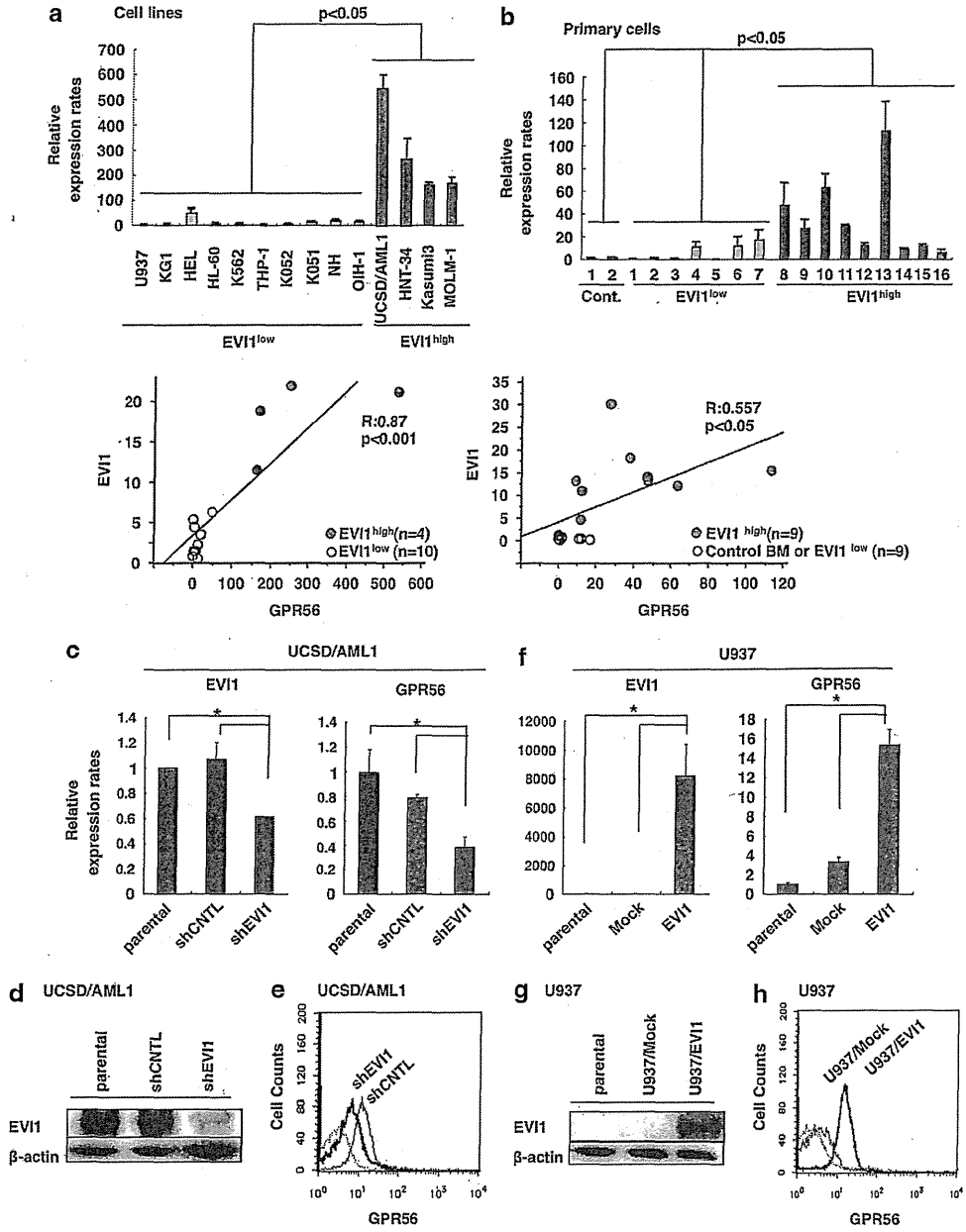

Figure 1. GPR56 is highly expressed in EVI1^{high} leukemia cells. (**a**) *GPR56* was detected in 14 AML cell lines, including 10 EVI1^{low} and 4 EVI1^{high} AML cell lines, using quantitative real-time PCR. The data are shown as the fold change in *GPR56* mRNA expression (normalized to β-actin) relative to *GPR56* expression in U937 cells. The data are presented as the means ± s.d.. The lower figure shows the correlation between the expression of EVI1 and GPR56 in the EVI1^{high} and EVI1^{low} AML cell lines based on quantitative real-time PCR analysis. The significance of the differences among the groups was assessed via a two-tailed Student's *t*-test. (**b**) *GPR56* was detected in 16 primary AML cell samples, including seven EVI1^{low} and nine EVI1^{high} AML samples. Two BM samples from healthy volunteers were used as controls. The data are shown as the fold changes in *GPR56* mRNA expression (normalized to β-actin) relative to the *GPR56* expression in control BM cells (no. 1). The data are presented as the means ± s.d. The lower figure shows the correlation between the expression of EVI1 and GPR56 in EVI1^{high} and EVI1^{low} primary AML cells and control BM samples based on quantitative real-time PCR analysis. The significance of the differences among the groups was assessed via a two-tailed Student's *t*-test. (**c**) Introduction of the small hairpin RNA (shRNA) expression vector specific for EVI1 into UCSD/AML1 cells with EVI1^{high} expression decreased GPR56 expression. Quantitative real-time reverse-transcription PCR (RT-PCR) analysis of EVI1 and GPR56 was performed in parental cells, shCNTL cells, and shEVI1 cells. The data were normalized to β-actin and are presented as relative fold changes compared with the expression in parental UCSD/AML1 cells. The data are presented as the means ± s.d. (**d**) The expression of EVI1 was downregulated in the UCSD/AML1/shEVI1 cells. EVI1 protein expression in parental UCSD/AML1, UCSD/AML1/shCNTL and UCSD/AML1/shEVI1 cells was detected using an anti-EVI1 antibody. (**e**) The cell surface expression of GPR56 in UCSD/AML1/shCNTL and UCSD/AML1/shEVI1 cells was detected by flow cytometric analysis. (**f**) The induction of GPR56 expression by forced expression of EVI1 in U937 cells expressing EVI1^{low} is shown. Quantitative real-time RT-PCR analysis of EVI1 and GPR56 was performed in parental U937 cells, U937/Mock cells and U937/EVI1 cells. The data were normalized to β-actin and are presented as relative fold changes compared with the expression in parental U937 cells. The data are presented as the means ± s.d. (**g**) EVI1 protein expression in parental U937 cells, U937/Mock cells and U937/EVI1 cells was detected with an anti-EVI1 antibody. (**h**) The cell surface expression of GPR56 in U937/Mock cells and U937/EVI1 cells was detected by flow cytometric analysis.

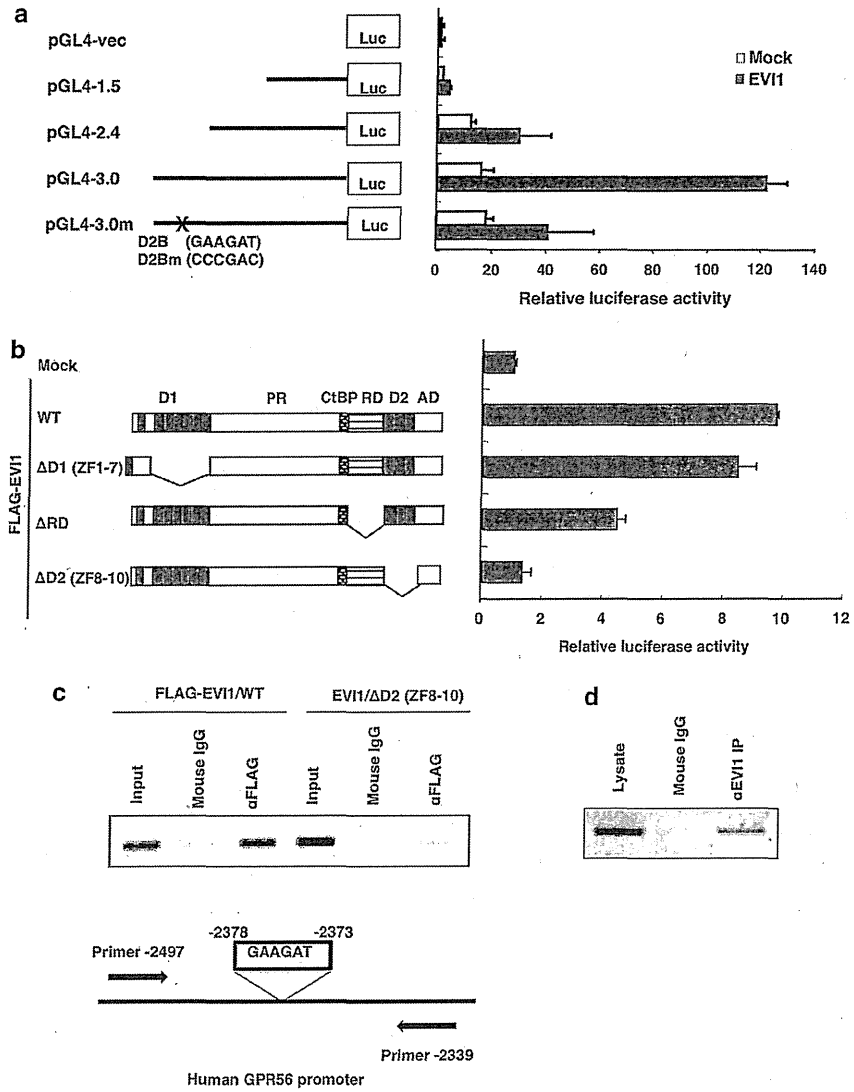

Figure 2. EVI1 binds to the promoter region of GPR56 to enhance its expression. (**a**) Structures of the GPR56 promoter region reporter plasmids are shown. A 1.5, 2.4 or 4.0 kb fragment of the GPR56 promoter region or a 4.0 kb fragment, in which GAAGAT was replaced with CCCGAC in the second ZF domain-binding sequence between −4.0 to −2.4 kb, was inserted upstream of the luciferase gene in the reporter plasmid pGL4. A mock reporter plasmid (pGL4-Vec) was used as a control. The fold change in promoter activity is shown as the ratio of normalized luciferase activity to the activity following control pGL4-Vec transfection. The open columns display the promoter activities of the various reporter plasmids, and the closed columns display the activities of a reporter plasmid in the presence of an EVI1 expression vector. All luciferase reporter assays were performed in duplicate in two independent experiments. The values and error bars depict the means ± s.d. (**b**) The structures of wild-type EVI1 and the EVI1 mutants with a series of deleted domains are depicted. COS7 cells were co-transfected with the GPR56 reporter vector, and each expression vector was co-transfected with EVI1 or EVI1 mutants (ΔD1 (ZF1-7), ΔRD, or ΔD2 (ZF8-10)). The fold change was calculated by dividing the fold activation of each EVI1 mutant co-transfected with pGL4-3.0 by the fold activation of the respective EVI1 mutant co-transfected with pGL4-vec. All of the luciferase reporter assays were performed in duplicate in two independent experiments. The values and error bars depict the means ± s.d. (**c**) Chromatin immunoprecipitation analysis of the EVI1-binding site in the GPR56 promoter region after transfection with the EVI1 expression vector is shown. After co-transfection with FLAG-tagged EVI1/WT or EVI1/ΔD2 (ZF8-10) with pGL4-3.0, formalin-fixed DNA fragments were immunoprecipitated with an anti-FLAG antibody or control mouse immunoglobulin G. The precipitated DNA was then amplified using specific primers to detect the EVI1-binding sites. (**d**) Chromatin immunoprecipitation of the endogenous EVI1 protein from UCSD/AML1 cells is shown. Formalin-fixed DNA fragments were immunoprecipitated with an anti-EVI1 antibody or control mouse immunoglobulin G. The precipitated DNA was then amplified using specific primers to detect the EVI1-binding sites.

cells with high or low GPR56 expression. After introduction of GPR56-specific small hairpin RNA or control small hairpin RNA into UCSD/AML1 cells, the expression of GPR56 was significantly decreased in UCSD/AML1/shGPR56 cells compared with the UCSD/AML1/shCNTL cell line (Figures 3a and b). The cellular adhesion of these lines was evaluated using either a feeder layer consisting of a murine osteoblastic cell line, MC3T3-E1, or using plates coated with fibronectin, Matrigel, laminin-1 or collagen type III. The adhesion of UCSD/AML1/shGPR56 cells to MC3T3-E1 cells and the various types of extracellular matrix was significantly impaired compared with that of the parental and UCSD/AML1/shCNTL cells (Figure 3c). Similar results were obtained for PT9 cells

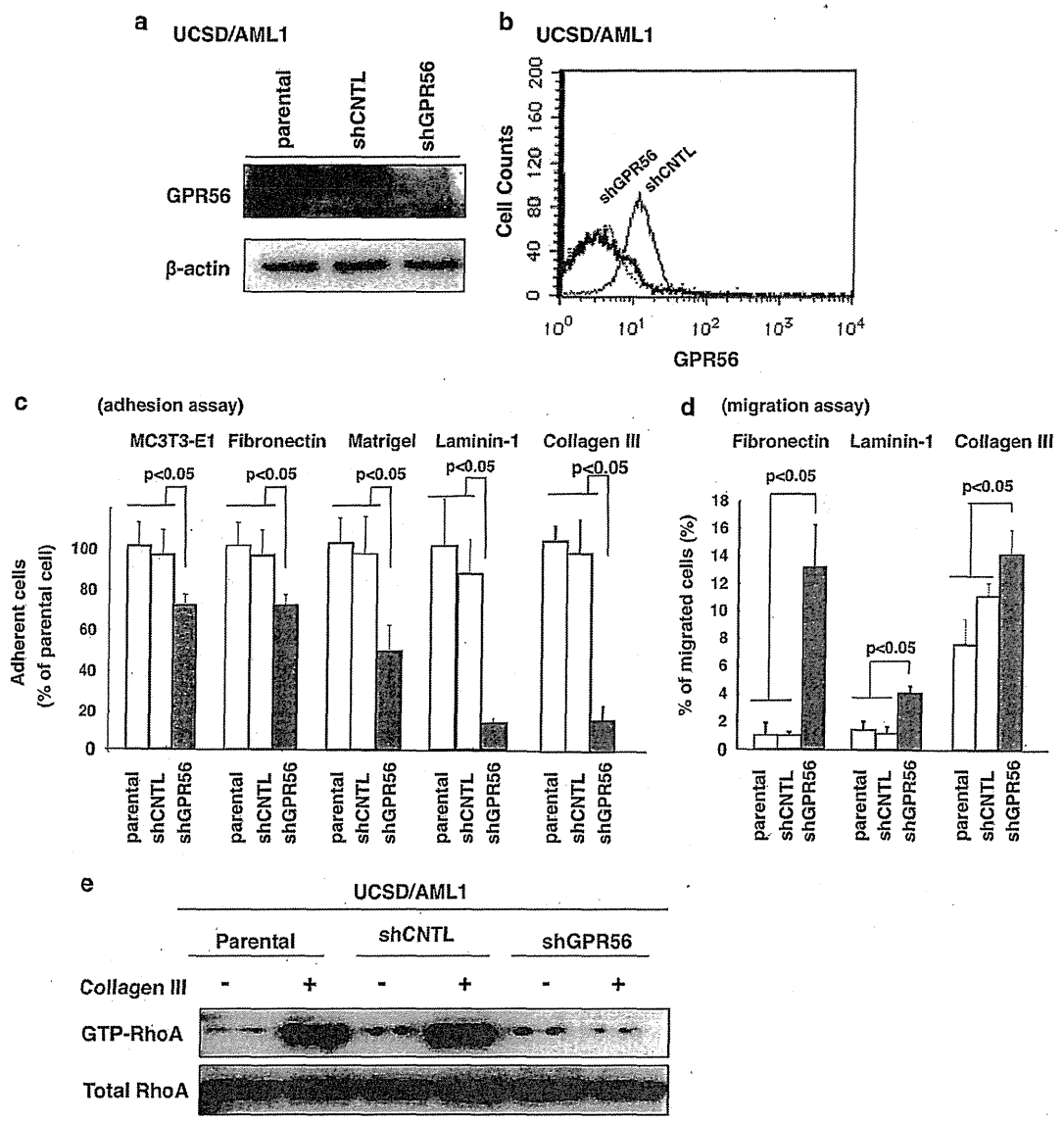

Figure 3. Knockdown of GPR56 expression increases the cell migration ability and decreases cellular adhesion to the extracellular matrix (ECM) through activation of the RhoA pathway. (**a**) Introduction of the shGPR56 expression vector into UCSD/AML1 cells downregulated GPR56 protein expression. The expression of GPR56 in parental UCSD/AML1, UCSD/AML1/shCNTL and UCSD/AML1/shGPR56 cells was detected with an anti-GPR56 antibody. (**b**) The cell surface expression of GPR56 in UCSD/AML1/shCNTL and UCSD/AML1/shGPR56 cells was determined by flow cytometric analysis. (**c**) The adhesion of parental UCSD/AML1, UCSD/AML1/shCNTL and UCSD/AML1/shGPR56 cells to MC3T3-E1 or ECM (fibronectin, Matrigel, laminin-1 or collagen type III) was quantified. The data are presented as the means ± s.d of the relative fold changes compared with the adherent cells in parental UCSD/AML1 cells. (**d**) The migration activities of the parental UCSD/AML1, UCSD/AML1/shCNTL and UCSD/AML1/shGPR56 cells through an ECM layer of fibronectin, laminin-1 or collagen type III were measured in response to an stromal cell-derived factor-1 (SDF-1α) gradient. The percentages of migrated cells are shown compared with the total cell numbers in this experiment. The data are presented as the means ± s.d. (**e**) The activated form of RhoA in parental UCSD/AML1, UCSD/AML1/shCNTL and UCSD/AML1/shGPR56 cells was measured via western blot analysis. The level of total RhoA in the cell lysates served as an internal control.

transfected with shGPR56 (PT9/shGPR56) (Supplementary Figures 3a and b). By contrast, the adhesion of U937/GPR56 cells was significantly increased compared with that of the parental and U937/Mock cells (Supplementary Figures 3c and d). To determine the cell migration abilities of the leukemia cells, the cells were added to the upper well of a Boyden chamber after fibronectin, laminin-1 or collagen type III had been embedded at the interface, and culture medium containing stromal cell-derived factor-1 was added to the bottom chamber. The number of migrating UCSD/AML1/shGPR56 cells was significantly increased compared with that of the parental and UCSD/AML1/shCNTL cells in the three different types of coated chambers (Figure 3d). Because the expression of CXCR4 was not significantly different between both cell types (Supplementary Figure 4), the increased migration ability mainly depended on the adhesion ability of the cells to the extracellular matrix in a Boyden chamber.

Collagen type III and other extracellular matrix molecules induce activation of the small GTP-binding protein RhoA downstream of GPR56;[31] therefore, we next determined the protein levels of GTP-bound RhoA in these cell lines. The level of GTP-bound RhoA in

parental and UCSD/AML1/shCNTL cells was increased after stimulation by collagen type III. However, the GTP-bound RhoA content in nonstimulated AML/shGPR56 cells was lower than the content in control cell lines, and stimulation with collagen type III did not increase the amount of GTP-bound RhoA in AML/shGPR56 cells (Figure 3e). To confirm whether activation of RhoA is necessary for the cellular adhesion of AML cells showing high GPR56 expression, Y-27632, a selective inhibitor of the Rho-associated protein kinase p160ROCK, was added to the culture medium of UCSD/AML1 cells. In control medium, UCSD/AML1 cells attached to conventional culture plates with a spindle-shaped cell morphology. However, the morphology of UCSD/AML1 cells changed from dendritic to small and round after the treatment with Y-27632 (Supplementary Figure 5a). In addition, the adhesion of UCSD/AML1 cells to MC3T3-E1 cells or to fibronectin was significantly decreased by treatment with Y-27632 (Supplementary Figure 5b). Therefore, the high level of cellular adhesion of EVI1^{high} AML cells was partially dependent on the expression of GPR56, and downstream RhoA activation has an important role in regulating cellular adhesion and cell migration in EVI1^{high} AML cells.

Involvement of GPR56 expression in apoptosis of EVI1^{high} AML cells

In the next set of experiments, we determined whether the expression of GPR56 affects the growth and viability of EVI1^{high} AML cells. After infection of recombinant shGPR56- or shCNTL-containing lentivirus into EVI1^{high} UCSD/AML1 and EVI1^{high} HNT34 cells, greater than 90% of the infected cells were GFP positive. Cell growth was determined immediately after infection. The growth rates of both cell lines transduced with shGPR56 (UCSD/AML1/shGPR56 and HNT34/shGPR56) were significantly decreased 3–5 days after infection compared with the growth rates of parental and shCNTL-infected cells (Figures 4a and b). Moreover, after introduction of the shGPR56 expression vector into PT9 cells, the colony-forming ability of parental PT9, PT9/shCNTL and PT9/shGPR56 cells was determined in methylcellulose cultures with GM- colony-stimulating factor. The colony number and size of granulocyte/macrophage colony-forming units were significantly reduced in PT9/shGPR56 cells (Supplementary Figures 6a and b). Therefore, we next determined whether apoptotic cell death was induced in shGPR56 cells. In a cell cycle analysis, an increase in the SubG1-phase cell population was observed in the UCSD/AML1/shGPR56 cells (Figure 4c). To confirm the induction of apoptotic cell death by GPR56 knockdown, lentivirus-infected cells were analyzed via flow cytometry after double staining with 7-Aminoactinomycin D and phycoerythrin-conjugated Annexin V (Figures 4d and e). The population of apoptotic cell death in the UCSD/AML1/shGPR56 cells was significantly increased compared with that in the UCSD/AML1/shCNTL cells several days after lentiviral infection, suggesting that the apoptosis of the UCSD/AML1/shGPR56 cells was due to the reduction of GPR56 expression. To determine the molecular mechanism underlying the inhibition of the apoptosis pathway downstream of GPR56 signaling, we determined the protein expression status of known apoptotic indicators and cell cycle regulators, including p53 and caspase-3 (Figure 4f). Cleaved caspase-3 fragments were detected in UCSD/AML1/shGPR56 cells, indicating that the apoptotic pathway was activated. Interestingly, the protein levels of p53, p21 and p27 were increased in UCSD/AML1/shGPR56 cells, whereas the level of MDM2 was proportionally decreased. However, the mRNA levels of p53 and MDM2 were unchanged in UCSD/AML1/shGPR56 cells compared with control UCSD/AML1 cells (Supplementary Figure 7), suggesting that an unknown signaling pathway downstream of GPR56 may stabilize the level of the MDM2 protein in EVI1^{high} AML cells, which promotes cell survival by promoting p53 degradation.

GPR56 expression was related to cell adhesion mediated drug resistance and the invasion ability of leukemic cells in BM

We next examined the role of GPR56 expression in the drug sensitivity of the cells to anticancer drugs. The UCSD/AML1 cells were seeded on MC3T3-E1 or BSA with various concentrations of Ara-C or daunorubicin (DNR) in culture media. Twenty-four hours after incubation, the percentages of surviving UCSD/AML1/shGPR56 cells on MC3T3-E1 cells (adherent status) were significantly reduced compared to the control UCSD/AML1 cells; however, the percentages of the UCSD/AML1/shGPR56 cells that survived under conventional culture condition were not different between the cells (Figures 5a and b). To determine the role of GPR56 expression in drug resistance *in vivo*, we performed xenotransplantation experiments of leukemia cells with high or low GPR56 expression into non-obese diabetic-severe combined immunodeficiency/γcnull (NOD-SCID/γcnull, NOG) mice. Initially, we determined the percentages of invaded leukemia cells in various organs two weeks after transplantation. Leukemia cells with high GPR56 expression (K562/GPR56 and UCSD/AML1) had a tendency to infiltrate into the BM more than other organs; however, leukemia cells with low GPR56 expression (K562/Mock and UCSD/AML1/shGPR56) infiltrated to the PB and other organs more than the BM (Figures 5c and d). To find the different effects of anticancer drugs on leukemia cells with high or low expression of GPR56 *in vivo*, mice transplanted with UCSD/AML1/shCNTL or UCSD/AML1/shGPR56 leukemia cells were treated with Ara-C for two weeks; at this time, the number of viable leukemia cells was determined in various organs by flow cytometry. The result showed that the USCD/AML1/shGPR56 cells were more effectively eliminated in the PB and spleen than in the BM (Figure 5e). Although we did not determine the survival curve of xenotransplanted mice undergoing anticancer treatment, the reduction of GPR56 expression in leukemia cells may help to enhance the sensitivity to anticancer drugs; further studies are needed to examine these effects.

High GPR56 expression in murine hematopoietic stem cell fractions and decreased numbers of HSCs in the BM of *Gpr56*$^{-/-}$ mice

Because GPR56, regulated by EVI1, is speculated to have an important function in the maintenance of HSCs, we next examined the expression of GPR56 in myeloid lineage cells at various stages of differentiation via flow cytometry analysis. Over 90% of LSK (Lin$^-$Sca-1$^+$c-Kit$^+$) cells expressed GPR56 on their cell surfaces, and more primitive self-renewing HSCs, including long-term and short-term HSCs, showed expression rates greater than 95% (Supplementary Table 3 and Supplementary Figure 8a). The level of GPR56 expression gradually decreased during the myeloid differentiation stages, and less than 50% of Lin$^+$ progenitor cells exhibited detectable GPR56 expression. In the BM in the diaphysis of tubular bones, high numbers of GPR56-positive cells were detected by fluorescence staining close to the periosteal rim, which is a region that contains potential BM osteosteal niches. The GPR56-positive mononuclear cells frequently coexpressed c-Kit and Sca-1, suggesting that GPR56$^+$c-Kit$^+$ primitive cells may localize near the periosteal region (Figure 6a and Supplementary Figure 8b). To determine the role of GPR56 in the regulation of hematopoiesis, we initially confirmed the downregulation of GPR56 expression in Lin$^-$ BM cells in *Gpr56*$^{-/-}$ mice (Supplementary Figure 9a), and determined the hematological profiles in their PB. There were no differences in the blood cell counts or hemoglobin content between the wild-type and *Gpr56*$^{-/-}$ mice (Supplementary Table 4). There were also no differences in whole-BM cells and spleen cells (Supplementary Figure 9b). Interestingly, the percentages of LSK cells in the BM were significantly decreased, but the percentages in the spleen and the PB were conversely increased in the *Gpr56*$^{-/-}$ mice

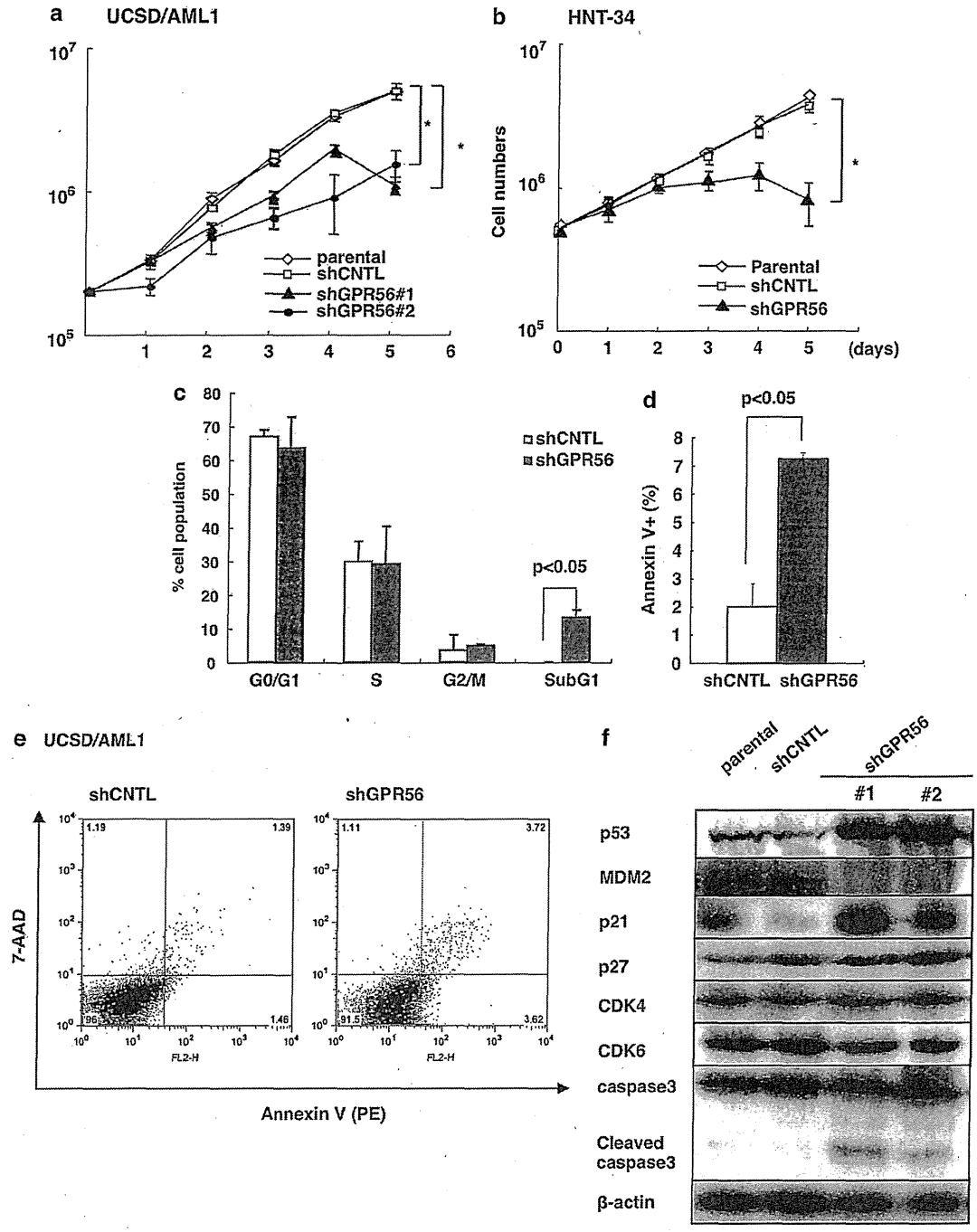

Figure 4. Knockdown of GPR56 expression induced apoptosis in EVI1^{high} leukemia cells through the accumulation of p53. (**a** and **b**) The influence of GPR56 knockdown on cell proliferation is shown. The growth rates of parental UCSD/AML1, UCSD/AML1/shCNTL and UCSD/AML1/shGPR56 cells and parental HNT34, HNT34/shCNTL and HNT34/shGPR56 cells were evaluated with the trypan blue exclusion assay. The live cells were counted after trypan blue staining using light microscopy. The data are presented as the means ± s.d. (**c**) Cell cycle fractions were analyzed by fluorescence-activated cell sorting after propidium iodide staining. The data are presented as the means ± s.d. (**d** and **e**). Six days after cell culture, UCSD/AML1/shCNTL and UCSD/AML1/shGPR56 cells were labeled with Annexin V and 7-aminoactinomycin D (7-AAD) and analyzed by flow cytometry. The percentages of Annexin V-stained dead cells are displayed as a bar graph (**d**), and the biparametric histogram represents the apoptotic cells, which show high Annexin V and low 7-AAD signals, and the secondary necrotic cells, which show high Annexin V and high 7-AAD signals (**e**). The experiments were performed in triplicate and repeated independently at least three times. (**f**) The expression of a series of apoptosis-related proteins was analyzed in various types of UCSD/AML1 cells by western blotting. Knockdown of GPR56 induced the accumulation of p53 by reducing the level of MDM2.

(Figures 6b and c). Moreover, the populations of short-term HSCs and long-term-HSCs were significantly reduced among the BM cells of the *Gpr56*$^{-/-}$ mice (Figure 6d). In the next experiment, we determined the colony-forming ability of mononuclear cells from the BM, spleen, liver and PB using semi-solid culture with several specific cytokines (Figure 6e). The number of granulocyte/

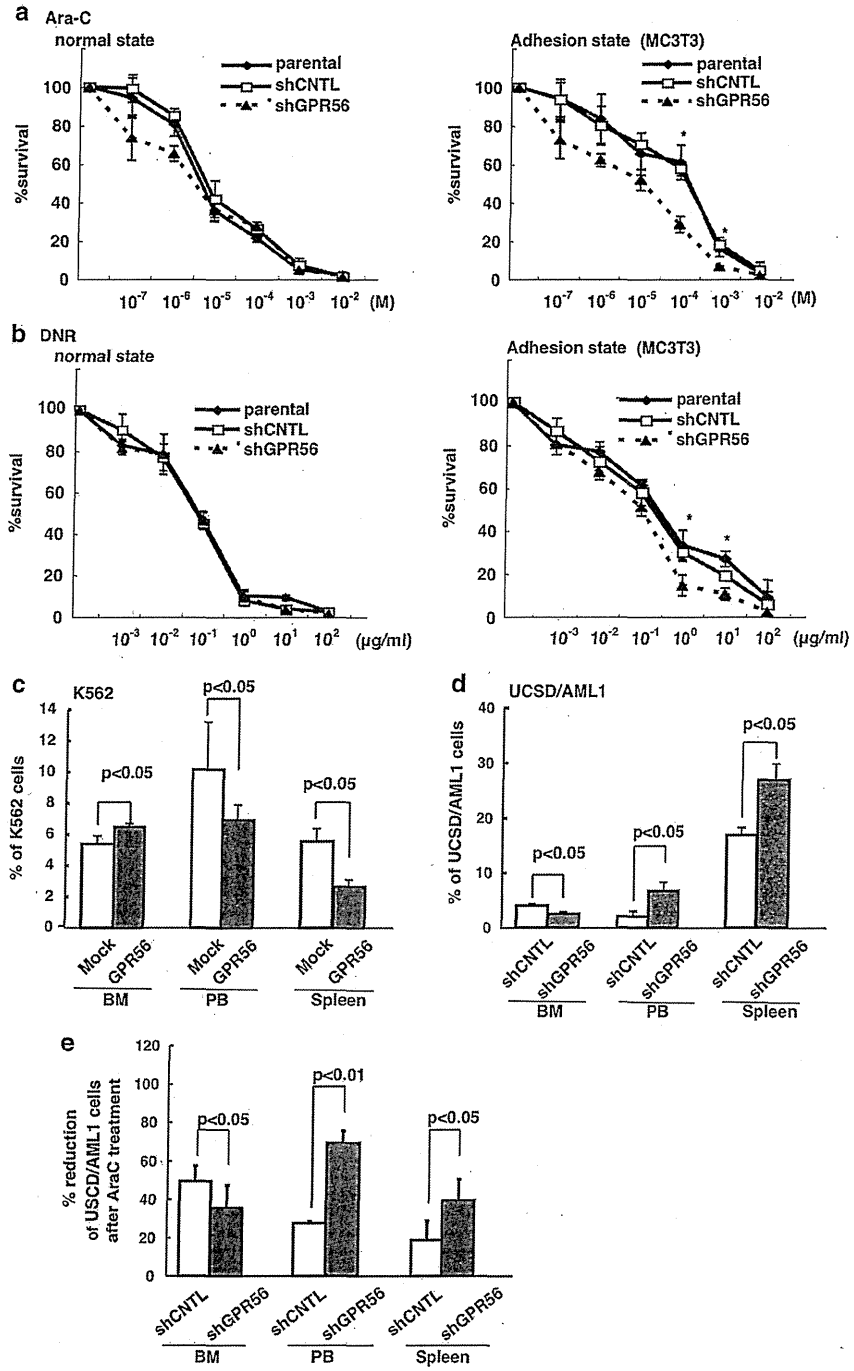

Figure 5. Knockdown of GPR56 inhibits drug resistance in AML cells, and GPR56 is an important regulator of leukemic cell engraftment. (**a** and **b**) The effect of adhesion on the chemosensitivity of UCSD/AML1, UCSD/AML1/shCNTL and UCSD/AML/shGPR56 cells is shown. UCSD/AML1 cells were incubated with Ara-C (**a**) or DNR (**b**) on MC3T3 coated plates. The number of viable cells and percentage of viable cells were assessed by trypan blue exclusion. The data are presented as the means ± s.d. Asterisks denote $P<0.05$ by Student's *t*-test. (**c**) K562/Mock cells or K562/GPR56 cells were intravenously transplanted into non-obese diabetic-severe combined immunodeficiency/γcnull (NOD-SCID/γcnull, NOG) mice. Two weeks after transplantation, the mice were killed, and the percentage of migration was analyzed. The means ± s.e. ($N=5$ per group), as evaluated by Student's *t*-test, are shown. (**d**) UCSD/AML1/shCNTL cells or UCSD/AML1/shGPR56 cells were intravenously transplanted into NOG mice. Two weeks after transplantation, the mice were killed, and the percentage of migration was analyzed. The means ± s.e. ($N=5$ per group), as evaluated by Student's *t*-test, are shown. (**e**) Mice were treated with Ara-C intravenously once per week (150 mg/kg). Two weeks after being treated with Ara-C, the mice were killed, and the percentage of the reduction in the leukemia cells was analyzed.

macrophage colony-forming units was significantly decreased in the BM of *Gpr56*$^{-/-}$ mice. However, granulocyte/macrophage colony-forming units and granulocyte, erythrocyte, monocyte/macrophage, megakaryocyte colony-forming unit (CFU-GEMM) numbers were clearly increased in the spleen, liver and PB of *Gpr56*$^{-/-}$ mice. Because the total colony numbers of

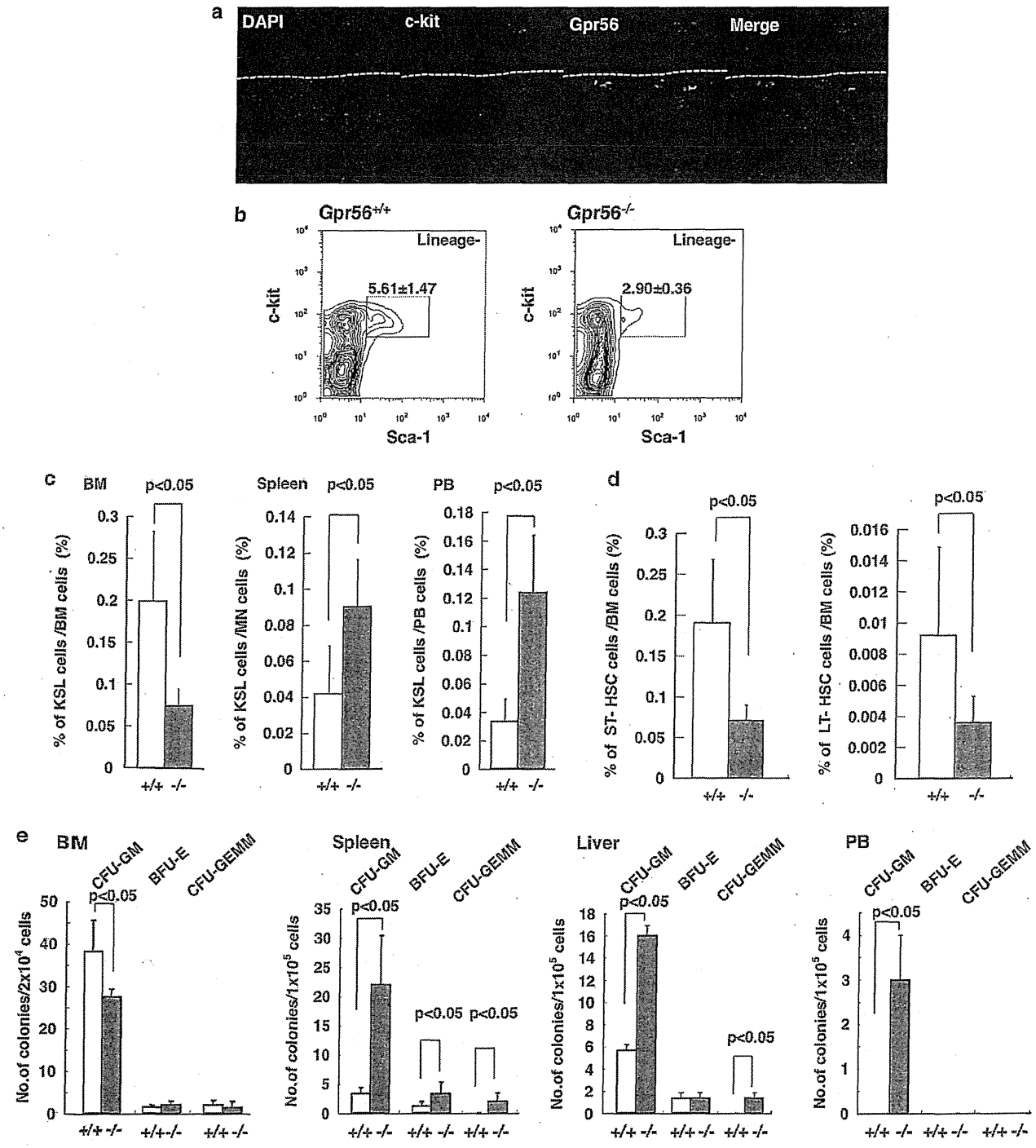

Figure 6. Decreased populations of HSCs in the BM of *Gpr56*$^{-/-}$ mice. (**a**) BM sections from wild-type mice were stained with 4′,6-diamidino-2-phenylindole (blue), c-Kit (red) and Gpr56 (white). c-Kit^{+}Gpr56^{+} cells resided near the periosteal region in the BM. (**b**) Populations of LSK cells were detected by flow cytometry and were isolated from the BM of 8-to 12-week-old wild-type (*Gpr56*$^{+/+}$) and *Gpr56*$^{-/-}$ mice (*Gpr56*$^{-/-}$). Data are presented as the mean percentages ± s.d. of LSK cells ($n = 5$). (**c**) The percentages of LSK cells per total mononuclear cell (MNC) counts in the BM from two legs (left side), the spleen (middle) and the PB (right side) are shown as white bars (+/+) and gray bars (−/−). The proportion of LSK cells in the BM of *Gpr56*$^{-/-}$ mice was significantly decreased, whereas those proportions in the spleen and PB were significantly increased. The data shown are the mean percentages of LSK cells ($n = 5$). (**d**) The population of short-term (left side) and long-term (LT) HSCs (right side) are shown as white bars (+/+) and gray bars (−/−). (**e**) The colony-forming abilities of MNCs from the BM, PB, spleens and livers of *Gpr56*$^{+/+}$ (+/+, white bar) and *Gpr56*$^{-/-}$ (−/−, gray bar) mice were determined in methylcellulose cultures by measuring granulocytes/monocytes colony-forming units(CFU-GM), erythroids (burst-forming unit-erythroid, BFU-E) and granulocytes/erythroids/monocytes/megakaryocytes (CFU-GEMM). The data shown are the mean numbers of colonies ($n = 3$).

granulocyte/macrophage colony-forming units were maintained in Gpr56$^{-/-}$ mice, the numbers of white blood cells were most likely not decreased in Gpr56$^{-/-}$ mice. Therefore, a part of the HSCs in *Gpr56*$^{-/-}$ mice do not remain in the BM and relocate to the peripheral organs where they maintain their differentiation capacity.

Decreased cellular adhesion and increased cellular migration ability in HSCs from *Gpr56*$^{-/-}$ mice

To investigate whether the decreased number of HSCs in the BM is related to a reduction in their adhesion and acquisition of migration ability, we assessed cellular adhesion and the cell migration ability using BM precursor cells with the Lin$^-$c-Kit$^+$

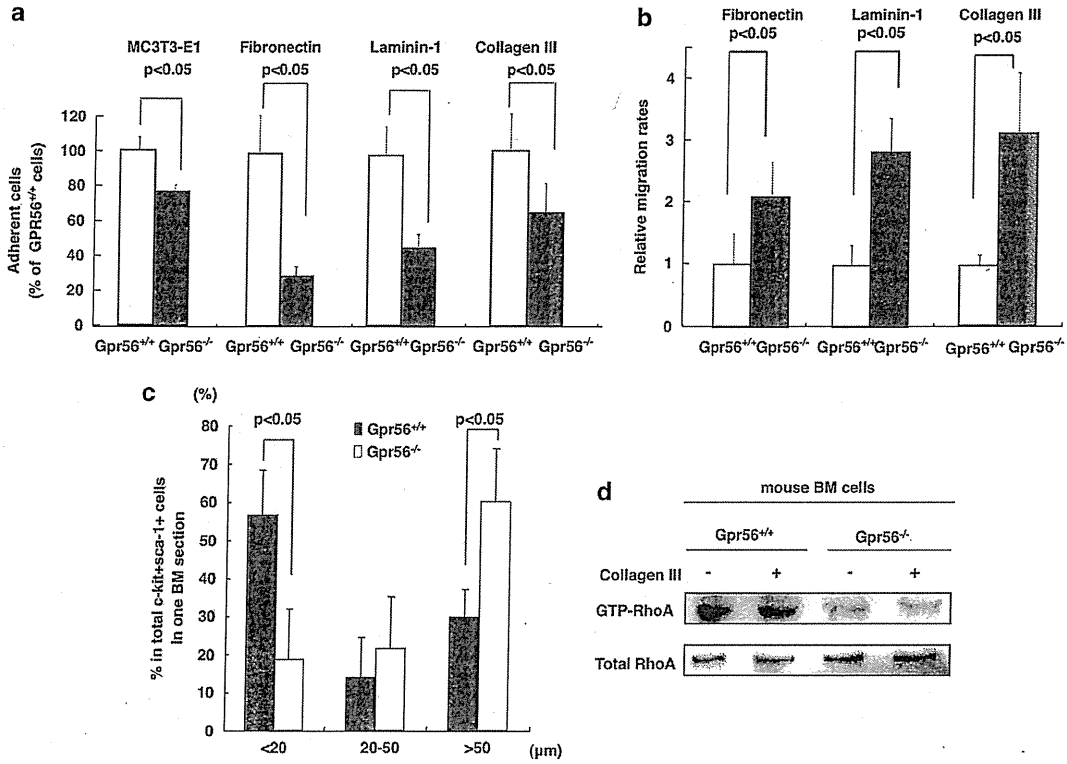

Figure 7. Increased migration and decreased cellular adhesion to the ECM of hematopoietic stem/progenitor cells from *Gpr56*$^{-/-}$ mice is induced through the RhoA pathway. (**a**) The adhesion of BM Lin$^-$c-Kit$^+$ (KL) cells from *Gpr56*$^{+/+}$ or *Gpr56*$^{-/-}$ mice to MC3T3-E1 adherent cells and three different types of ECM (fibronectin, laminin-1 or collagen type III) was measured, and the results are displayed as white bars (*Gpr56*$^{+/+}$) or gray bars (*Gpr56*$^{-/-}$). The strength of cellular adhesion is shown relative to the strength of KL cells from *Gpr56*$^{+/+}$ mice. The data are presented as the means ± s.d. ($n=3$) (**b**) The cellular migration of BM KL cells from wild-type or *Gpr56*$^{-/-}$ mice in response to an SDF-1α gradient is shown. Three different types of ECM interfaces (fibronectin, laminin-1 or collagen type III) were used in a Boyden chamber system in this experiment. The data are presented as the relative migration rates compared with the migration rates of KL cells from *Gpr56*$^{+/+}$ mice. The data are presented as the means ± s.d. ($n=3$) (**c**) The *in situ* localization of c-Kit$^+$ and Sca-1$^+$ cells within the femur BM of *Gpr56*$^{+/+}$ or *Gpr56*$^{-/-}$ mice was detected by immunohistochemistry. The localization of c-Kit$^+$ and Sca-1$^+$ cells was categorized into three groups based on the distance from the periosteum (<20, 20–50 and >50 μm). The data are presented as the means ± s.d. ($n=3$). (**d**) The protein level of GTP-bound RhoA in Lin$^-$c-Kit$^+$ BM cells from *Gpr56*$^{+/+}$ or *Gpr56*$^{-/-}$ mice was measured by western blot analysis. The protein level of total RhoA in the cell lysates served as a control.

Figure 8. The expression of GPR56 in HSCs is involved in the maintenance of quiescence and LT BM reconstitution. (**a**) After collecting LSK cells labeled with Annexin V-PE and 7-AAD, the populations (%) of early apoptotic cells were counted using Annexin V$^+$ and 7-AAD$^-$ staining, and are displayed as white bars (*Gpr56*$^{+/+}$) or dark bars (*Gpr56*$^{-/-}$). The data are presented as the means ± s.d. ($n=3$). (**b**) Following bromodeoxyuridine (BrdU) incorporation *in vivo*, LSK cells from *Gpr56*$^{+/+}$ (white bar) and *Gpr56*$^{-/-}$ (gray bar) mice were isolated and stained with an allophycocyanin (APC)-conjugated anti-BrdU antibody and 7-AAD to analyze the cell cycle stage by flow cytometry. The data are presented as the means ± s.d. ($n=3$). (**c**) After staining LSK cells from *Gpr56*$^{+/+}$ (left) and *Gpr56*$^{-/-}$ mice (right) with Hoechst 33342 and pyronin Y, the populations (%) of LSK cells in the G0-phase of the cell cycle were assessed via flow cytometry. The data are presented as the means ± s.d. ($n=3$). (**d**) *Gpr56*$^{+/+}$ and *Gpr56*$^{-/-}$ mice were administered 5-fluorouracil intraperitoneally once per week for 2 weeks, and the survival of individual mice was monitored daily. The results were analyzed using a log-rank nonparametric test, and the survival rates of *Gpr56*$^{+/+}$ (solid line) and *Gpr56*$^{-/-}$ (dotted line) mice were plotted on a Kaplan–Meier curve ($n=6$). (**e**) For competitive repopulation assays, donor BM cells or LSK cells from CD45.2$^+$*Gpr56*$^{+/+}$ or *Gpr56*$^{-/-}$ mice were mixed in a 1:1 or 1:50 ratio with CD45.1$^+$ competitor cells and transplanted into lethally irradiated CD45.1$^+$-recipient mice. (**f** and **g**) The chimerism in the first transplantation was measured as the number of white blood cells from the PB (**f**) and as the number of lineage-negative c-Kit-positive cells from the BM (Lin$^-$c-Kit$^+$ BM) (**g**). (**h** and **i**) The chimerism in the second transplantation was measured as the number of white blood cells from the PB (**h**) and as the number of lineage-negative cells from the BM (Lin$^-$c-Kit$^+$ BM) (**i**) The data shown are the mean percentages ± s.d. of donor-derived cells in the PB at 4 weeks after transplantation ($n=5$). The chimerism in Lin$^-$c-Kit$^+$ BM cells was determined by flow cytometry 16 weeks post-transplantation ($n=5$). (**j** and **k**) LSK cells from CD45.2$^+$ wild-type or *Gpr56*$^{-/-}$ mice were used for a competitive repopulation assay. The chimerism in the transplantation was measured as the number of white blood cells from the PB (**j**) and as the number of lineage-negative c-Kit-positive cells from the BM (Lin$^-$c-Kit$^+$ BM) (**k**). The data shown are the mean percentages ± s.d. of donor-derived cells in the PB at 4 weeks after transplantation ($n=4$).

phenotype. The BM precursor cells in *Gpr56*$^{-/-}$ mice displayed decreased adhesion to MC3T3-E1 cells, fibronectin, laminin-1 and collagen type III as extracellular matrices (Figure 7a). The ability of BM precursor cells from *Gpr56*$^{-/-}$ mice to migrate towards the chemoattractant stromal cell-derived factor-1 was significantly increased on the three types of coated extracellular matrices (Figure 7b). In the next experiment, we determined the precise localization of HSCs in the BM using confocal microscopy after staining BM sections with phycoerythrin-conjugated c-kit and fluorescein isothiocyanate-conjugated Sca-1 antibodies. The

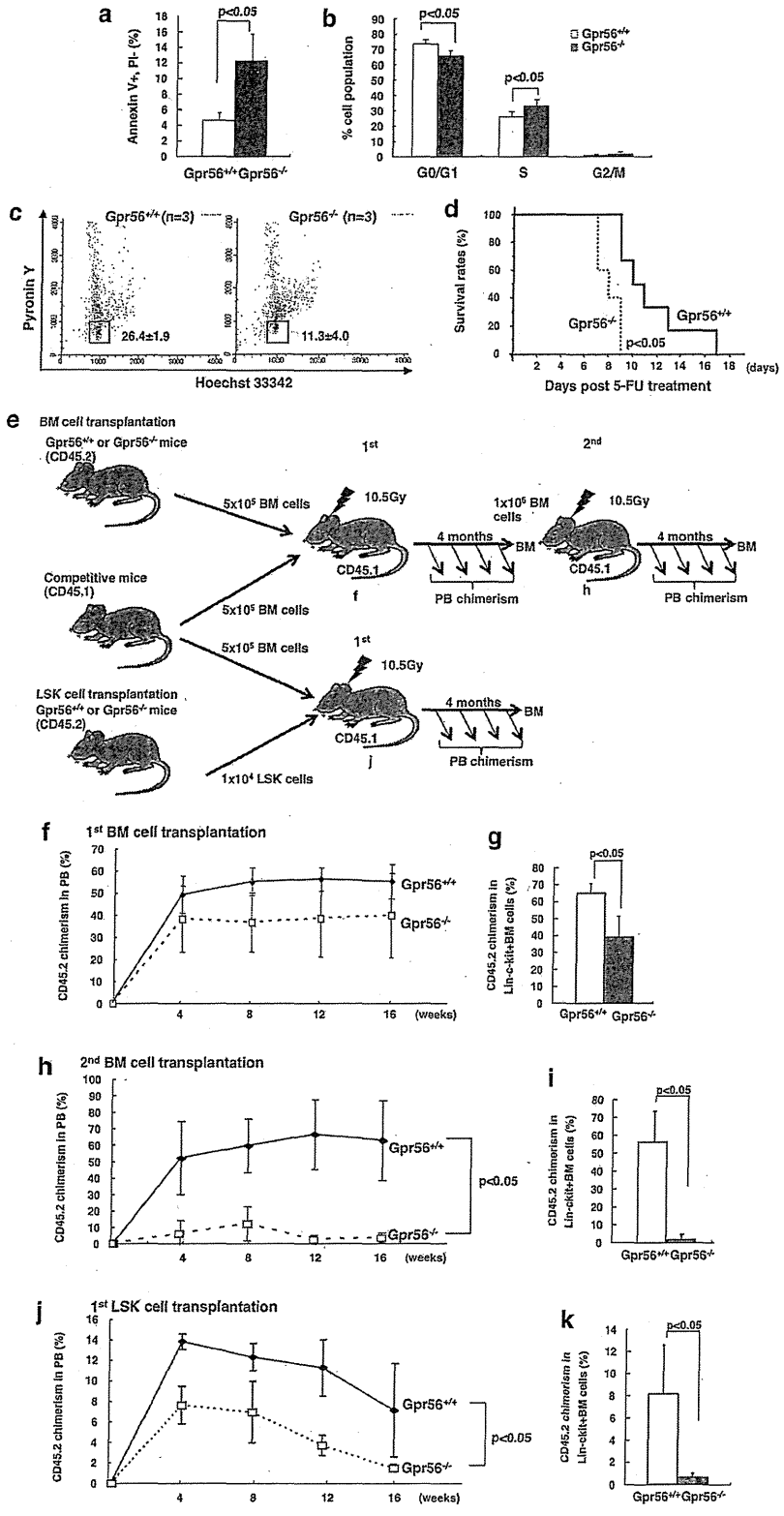

number of primitive cells located less than 20 μm from the periosteum was significantly decreased in the *Gpr56*$^{-/-}$ mice (Figure 7c and Supplementary Figure 10). By contrast, the number of cells that were located more than 50 μm from the periosteum was increased in the *Gpr56*$^{-/-}$ mice. Finally, to investigate whether the migration and adhesion abilities of HSCs depend on GPR56 signaling through the $G\alpha_{12/13}$ and Rho signaling pathway, we determined the protein levels of GTP-bound RhoA in the HSC fractions of wild-type and *Gpr56*$^{-/-}$ mice (Figure 7d). High levels of GTP-bound RhoA accumulated in wild-type mice under both nonstimulated and collagen type III-stimulated conditions, although the stimulation mechanism was unknown in the HSC fraction of wild-type mice. Conversely, low levels of GTP-bound RhoA were detected in the *Gpr56*$^{-/-}$ mice in both the untreated and collagen type III-treated BM cells. In addition, the ability of HSCs to adhere to MC3T3-E1 cells or to fibronectin was significantly decreased by the treatment with Y-27632, a p160ROCK kinase inhibitor (Supplementary Figures 11a and b). Thus, the data suggest that the cellular adhesion of HSCs was decreased by the reduction of RhoA signaling activity, resulting in a reduction in HSCs near the periosteum.

The expression of GPR56 in HSCs was involved in the maintenance of quiescence and long-term BM reconstitution

Because the fraction of LSK cells in *Gpr56*$^{-/-}$ mice was decreased in the BM along with a reduction in their adhesion ability, we next investigated the fraction of apoptotic cells and cell cycle parameters in the LSK fraction in the BM. The Annexin V^{+}7-7-aminoactinomycin D^{-} fraction of apoptotic cells was significantly increased in *Gpr56*$^{-/-}$ mice (Figure 8a and Supplementary Figure 12). The population of G0/G1-phase cells was also decreased, together with an increased population of S-phase cells in the *Gpr56*$^{-/-}$ mice (Figure 8b). Furthermore, the population of G0-phase cells separated by pyronin Y and Hoechst 33342 staining was significantly reduced in the LSK fraction in *Gpr56*$^{-/-}$ mice compared with the population in wild-type mice (Figure 8c). In the next experiment, to determine the drug sensitivity of BM cells in the *Gpr56*$^{-/-}$ mice to an anticancer drug, 5-fluorouracil was injected at a dose of 150 mg/kg once per week for 2 weeks into each of six wild-type and *Gpr56*$^{-/-}$ mice (Figure 8d). The median lifespan of the wild-type mice was 10.5 days, whereas the lifespan of the *Gpr56*$^{-/-}$ mice was significantly shortened to 7.5 days ($P<0.05$); this result suggests that the reduction of the HSC population in the BM and the decreased proportion of G0-phase cells resulted in enhanced cytotoxicity in the *Gpr56*$^{-/-}$ mice in response to this anticancer drug. Finally, to define the ability of HSCs in the *Gpr56*$^{-/-}$ mice to reconstitute hematopoiesis, a mixture of CD45.2^{+} BM cells from wild-type or *Gpr56*$^{-/-}$ mice with CD45.1^{+} competitor BM cells was transplanted into lethally irradiated CD45.1^{+} mice (Figure 8e). In the first transplantation, the population of CD45.2^{+} white blood cells from *Gpr56*$^{-/-}$ mice in the PB was decreased in the recipients compared with the population in the wild-type mice (Figure 8f). Moreover, the population of myeloid, erythroid, megakaryocyte and Lin^{-}c-Kit^{+} BM cells from *Gpr56*$^{-/-}$ mice in the recipient BM was significantly decreased (Figure 8g and Supplementary Figure 13). In the second transplantation, the population of white blood cells from *Gpr56*$^{-/-}$ mice was significantly diminished in the PB and Lin^{-}c-Kit+ BM cell fractions of the recipients (Figures 8h and i).

Furthermore, to confirm the reduced reconstitution ability of the stem cell fraction in the *Gpr56*$^{-/-}$ mice, we transplanted 1×10^{4} LSK cells from wild-type or *Gpr56*$^{-/-}$ mice with CD45.1^{+} competitor BM cells into lethally irradiated CD45.1^{+} mice. As shown in Figures 8j and k, the population of white blood cells from *Gpr56*$^{-/-}$ mice was significantly decreased in the PB and Lin^{-}c-Kit+ BM cell fractions of the recipients. Thus, the reduction of cell numbers and the depletion of the quiescent cell population in BM-derived HSCs may result in a reduced capacity for HSC reconstitution in *Gpr56*$^{-/-}$ mice.

DISCUSSION

In this study, RhoA signaling through $G\alpha_{12/13}$ coupled with GPR56 is a novel signaling pathway for HSC maintenance in BM, which is regulated by EVI1. As high levels of GPR56 expression correlate with the cellular transformation phenotypes of several cancer tissues,[21–23] high expression of GPR56 in EVI1^{high} AML cells may result in apoptotic resistance with a poor prognosis.

Rac1/Rac2 and the Rho family GTPase Cdc42 previously have been implicated in the maintenance of HSCs through the regulation of adhesion, migration, homing and mobilization. HSCs from Cdc42-deficient mice exhibit impaired adhesion, homing, lodging and retention, leading to massive cellular egress from the BM to distal organs and PB, ultimately resulting in failure of engraftment.[25,29] Rac-1-deficient HSCs show a significant reduction in hematopoietic reconstitution, without any effect on cellular adhesion. However, Rac2-deficient HSCs exhibit decreased cellular adhesion but normal short-term engraftment, suggesting a prominent role for Rac2 in integrin-mediated stem cell adhesion.[26–28] On the other hand, P190-B RhoGAP is a major regulator of Rho GTPases, and abnormally high levels of active RhoA protein were detected in embryo-derived cells from P190-B-deficient mice. The migration and adhesion of hematopoietic progenitor cells from the P190-deficient mice were markedly enhanced in an *in vitro* experiment, and the high levels of active RhoA were associated with a significant enhancement of HSC engraftment and reconstitution *in vivo*.[32] In this study, we demonstrated that downregulation of GPR56 expression in EVI1^{high} leukemia cells and *Gpr56*$^{-/-}$ LSK cells caused RhoA inactivation with a concomitant decrease in cellular adhesion. Moreover, apoptotic cell death and decreased G0 cell fractions in leukemia cells and HSC cells with low RhoA activity were found in both *in vitro* and *in vivo* experiments, and the inactivation of RhoA activity in HSC cells from *Gpr56*-deficient mice reduced the reconstitution ability. On the basis of the findings of P190-B- and GPR56-deficient mice, the level of RhoA activation may significantly influence the maintenance of the HSCs in BM.

Rac is activated by the stimulation of CXCR4 by stromal cell-derived factor-1, by adhesion via β1 integrin, and by the stimulation of c-Kit by stem cell factors, all of which are involved in stem cell engraftment. However, no specific ligands of GPR56 other than collagen type III are currently known. Because the expression level of GPR56 was significantly higher in CD34^{+} CD38^{-}EVI1^{high} LSC fractions than in normal HSCs (Supplementary Figure 14), GPR56 has the potential to become a novel molecular target in EVI1^{high} leukemia. The results of this study have led to a significant improvement in our understanding of stem cell retention in BM and trafficking in the peripheral circulation. Furthermore, if the specific ligand of GPR56 is identified, we will be able to develop a small-molecule inhibitor or antibody as a specific therapeutic target for refractory leukemia that could modulate the adhesion, mobilization and proliferation abilities of EVI1^{high} leukemia cells.

CONFLICT OF INTEREST

The authors declare no conflict of interest.

ACKNOWLEDGEMENTS

We gratefully acknowledge Genentech for providing the *Gpr56* knockout mice for the studies. This work was supported by a grant-in-aid for the third term comprehensive 10-year strategy for cancer control from the Ministry of Health and Welfare; a grant-in-aid for scientific research from The Ministry of Education, Culture, Sports, Science and Technology; a grant-in-aid for scientific research from the Japan Society for the Promotion of Science; and a Grant-in-Aid for Scientific Research on Innovative Areas.

REFERENCES

1 Ishikawa F, Yoshida S, Saito Y, Hijikata A, Kitamura H, Tanaka S *et al.* Chemotherapy-resistant human AML stem cells home to and engraft within the bone-marrow endosteal region. *Nat Biotechnol* 2007; **25**: 1315–1321.

2 Lane SW, Scadden DT, Gilliland DG. The leukemic stem cell niche: current concepts and therapeutic opportunities. *Blood* 2009; **114**: 1150–1157.

3 Morishita K, Parker DS, Mucenski ML, Jenkins NA, Copeland NG, Ihle JN. Retroviral activation of a novel gene encoding a zinc finger protein in IL-3-dependent myeloid leukemia cell lines. *Cell* 1988; **54**: 831–840.

4 Morishita K, Parganas E, William CL, Whittaker MH, Drabkin H, Oval J *et al.* Activation of EVI1 gene expression in human acute myelogenous leukemias by translocations spanning 300–400 kilobases on chromosome band 3q26. *Proc Natl Acad Sci USA.* 1992; **89**: 3937–3941.

5 Lugthart S, Gröschel S, Beverloo HB, Kayser S, Valk PJ, van Zelderen-Bhola SL *et al.* Clinical, molecular, and prognostic significance of WHO type inv(3)(q21q26.2)/t(3;3)(q21;q26.2) and various other 3q abnormalities in acute myeloid leukemia. *J Clin Oncol* 2010; **28**: 3890–3898.

6 Barjesteh van Waalwijk van Doorn-Khosrovani S, Erpelinck C, van Putten WL, Valk PJ, van der Poel-van de Luytgaarde S, Hack R *et al.* High EVI1 expression predicts poor survival in acute myeloid leukemia: a study of 319 *de novo* AML patients. *Blood* 2003; **101**: 837–845.

7 Lugthart S, van Drunen E, van Norden Y, van Hoven A, Erpelinck CA, Valk PJ *et al.* High EVI1 levels predict adverse outcome in acute myeloid leukemia: prevalence of EVI1 overexpression and chromosome 3q26 abnormalities underestimated. *Blood* 2008; **111**: 4329–4337.

8 Groschel S, Lugthart S, Schlenk RF, Valk PJ, Eiwen K, Goudswaard C *et al.* High EVI1 expression predicts outcome in younger adult patients with acute myeloid leukemia and is associated with distinct cytogenetic abnormalities. *J Clin Oncol* 2010; **28**: 2101–2107.

9 Valk PJ, Verhaak RG, Beijen MA, Erpelinck CA, Barjesteh van Waalwijk van Doorn-Khosrovani S, Boer JM *et al.* Prognostically useful gene-expression profiles in acute myeloid leukemia. *N Engl J Med* 2004; **350**: 1617–1628.

10 Verhaak RG, Wouters BJ, Erpelinck CA, Abbas S, Beverloo HB, Lugthart S *et al.* Prediction of molecular subtype in acute myeloid leukemia based on gene expression profiling. *Haematologica* 2009; **94**: 131–134.

11 Eppert K, Takenaka K, Lechman ER, Waldron L, Nilsson B, van Galen P *et al.* Stem cell gene expression programs influence clinical outcome in human leukemia. *Nat Med* 2011; **17**: 1086–1093.

12 Yuasa H, Oike Y, Iwama A, Nishikata I, Sugiyama D, Perkins A *et al.* Oncogenic transcription factor Evi1 regulates hematopoietic stem cell proliferation through GATA-2 expression. *EMBO J.* 2005; **24**: 1976–1987.

13 Goyama S, Yamamoto G, Shimabe M, Sato T, Ichikawa M, Ogawa S *et al.* Evi-1 is a critical regulator for hematopoietic stem cells and transformed leukemic cells. *Cell Stem Cell* 2008; **3**: 207–220.

14 Saito Y, Nakahata S, Yamakawa N, Kaneda K, Ichihara E, Suekane A *et al.* CD52 as a molecular target for immunotherapy to treat acute myeloid leukemia with high EVI1 expression. *Leukemia* 2011; **25**: 921–931.

15 Yamakawa N, Kaneda K, Saito Y, Ichihara E, Morishita K. The increased expression of integrin α6 (ITGA6) enhances drug resistance in EVI1high leukemia. *PLoS ONE* 2012; **7**: e30706.

16 Ichihara E, Kaneda K, Saito Y, Yamakawa N, Morishita K. Angiopoietin1 contributes to the maintenance of cell quiescence in EVI1high leukemia cells. *BBRC* 2011; **416**: 239–245.

17 Piao X, Hill RS, Bodell A, Chang BS, Basel-Vanagaite L, Straussberg R *et al.* G protein-coupled receptor-dependent development of human frontal cortex. *Science* 2004; **303**: 2033–2036.

18 Li S, Jin Z, Koirala S, Bu L, Xu L, Hynes RO *et al.* GPR56 regulates pial basement membrane integrity and cortical lamination. *J Neurosci* 2008; **28**: 5817–5826.

19 Koirala S, Jin Z, Piao X, Corfas G. GPR56-regulated granule cell adhesion is essential for rostral cerebellar development. *J Neurosci* 2009; **29**: 7439–7449.

20 Iguchi T, Sakata K, Yoshizaki K, Tago K, Mizuno N, Itoh H. Orphan G protein-coupled receptor GPR56 regulates neural progenitor cell migration via a G alpha 12/13 and Rho pathway. *J Biol Chem* 2008; **283**: 14469–14478.

21 Shashidhar S, Lorente G, Nagavarapu U, Nelson A, Kuo J, Cummins J *et al.* GPR56 is a GPCR that is overexpressed in gliomas and functions in tumor cell adhesion. *Oncogene* 2005; **24**: 1673–1682.

22 Xu L, Begum S, Hearn JD, Hynes RO. GPR56, an atypical G protein-coupled receptor, binds tissue transglutaminase, TG2, and inhibits melanoma tumor growth and metastasis. *Proc Natl Acad Sci USA* 2006; **103**: 9023–9028.

23 Ke N, Sundaram R, Liu G, Chionis J, Fan W, Rogers C *et al.* Orphan G protein-coupled receptor GPR56 plays a role in cell transformation and tumorigenesis involving the cell adhesion pathway. *Mol Cancer Ther* 2007; **6**: 1840–1850.

24 Terskikh AV, Easterday MC, Li L, Hood L, Kornblum HI, Geschwind DH *et al.* From hematopoiesis to neuropoiesis: evidence of overlapping genetic programs. *Proc Natl Acad Sci USA* 2001; **98**: 7934–7939.

25 Yang FC, Atkinson SJ, Gu Y, Borneo JB, Roberts AW, Zheng Y *et al.* Rac and Cdc42 GTPases control hematopoietic stem cell shape, adhesion, migration, and mobilization. *Proc Natl Acad Sci USA* 2001; **98**: 5614–5618.

26 Cancelas JA, Lee AW, Prabhakar R, Stringer KF, Zheng Y, Williams DA. Rac GTPases differentially integrate signals regulating hematopoietic stem cell localization. *Nat Med* 2005; **11**: 886–891.

27 Gu Y, Filippi MD, Cancelas JA, Siefring JE, Williams EP, Jasti AC *et al.* Hematopoietic cell regulation by Rac1 and Rac2 guanosine triphosphatases. *Science* 2003; **302**: 445–449.

28 Ghiaur G, Lee A, Bailey J, Cancelas JA, Zheng Y, Williams DA. Inhibition of RhoA GTPase activity enhances hematopoietic stem and progenitor cell proliferation and engraftment. *Blood* 2006; **108**: 2087–2094.

29 Yang L, Wang L, Geiger H, Cancelas JA, Mo J, Zheng Y. Rho GTPase Cdc42 coordinates hematopoietic stem cell quiescence and niche interaction in the bone marrow. *Proc Natl Acad Sci USA* 2007; **104**: 5091–5096.

30 Ghiaur G, Ferkowicz MJ, Milsom MD, Bailey J, Witte D, Cancelas JA *et al.* Rac1 is essential for intraembryonic hematopoiesis and for the initial seeding of fetal liver with definitive hematopoietic progenitor cells. *Blood* 2008; **111**: 3313–3321.

31 Luo R, Jeong SJ, Jin Z, Strokes N, Li S, Piao X. G protein-coupled receptor 56 and collagen III, a receptor-ligand pair, regulates cortical development and lamination. *Proc Natl Acad Sci USA* 2011; **108**: 12925–12930.

32 Xu H, Eleswarapu S, Geiger H, Szczur K, Daria D, Zheng Y *et al.* Loss of Rho GTPase activating protein p190-B enhances hematopoietic stem cell engraftment potential. *Blood* 2009; **114**: 3557–3566.

Supplementary Information accompanies this paper on the Leukemia website (http://www.nature.com/leu)